Airborne Natural Source Electromagnetics Using an Arbitrary Base Station

Devin C. Cowan[1], Lindsey J. Heagy[2] and Douglas W. Oldenburg[3]
University of British Columbia

SUMMARY

The expensive and time-consuming nature of magnetotelluric (MT) surveys has motivated the development of airborne natural source EM (NSEM) systems, which includes Z-axis Tipper EM (ZTEM), quantum audio magnetotellurics (QAMT) and MobileMT. These systems compute transfer functions from airborne magnetic data, and horizontal field measurements at a base station located on the Earth's surface. Available literature offering in-depth analysis of the factors that influence airborne NSEM data and inversion results remains sparse; especially for systems that measure electric fields at the base station. In our work, we characterize the nature of QAMT data, and by extension MobileMT data. We demonstrate the impact of the conductivity at the base station on ZTEM and QAMT anomalies. And we investigate the impact of the starting and reference model on ZTEM and QAMT inversion results when the conductivity at the base station differs significantly from the host conductivity within the survey region. Our analysis determined that QAMT data are directly sensitive to the conductivity at the base station, and that QAMT anomalies are produced by anomalous magnetic fields arising from 3D structures within the survey region. Like ZTEM, models recovered through QAMT inversion depend significantly on the choice in starting and reference models. When the conductivity near the base station differs significantly from the background conductivity within the survey region, target structures are likely recovered erroneously. When the true host conductivity within the survey region is used as the starting and reference models, both ZTEM and QAMT inversions recover conductive and resistive structures appropriately regardless of base station conductivity. However, structures are also recovered near the base station. And these structures likely assist in fitting signatures produced by targets within the survey region, thus reducing our confidence in the recovered model.

Keywords: QAMT, ZTEM, inversion, airborne natural source EM

INTRODUCTION

Natural source electromagnetic (NSEM) methods have long been used to characterize the distribution of subsurface electrical conductivities (Tikhonov, 1950, Cagniard, 1953; Ward 1959; others). NSEM data are generated by computing the transfer functions that relate directional components of the Earth's natural magnetic (and electric) fields. Ground-based magnetotelluric (MT) data extract the most comprehensive information from the Earth's NSEM fields and are directly sensitive to subsurface conductivities (Cagniard, 1953). However, the expensive and time-consuming nature of MT surveys has motivated the development of airborne NSEM systems.

Airborne NSEM systems compute transfer functions from airborne magnetic data, and horizontal field measurements at a base station located on the Earth's surface. Z-axis Tipper EM (ZTEM) computes transfer functions from z-component airborne magnetic data and horizontal magnetic fields at a base station (Lo and Zang, 2008). Although much more economic than MT surveys, ZTEM data are collected within a relatively narrow frequency band (30 Hz - 720 Hz) and are only sensitive to contrasts in electrical conductivity across vertical interfaces. To economically collect MT-like impedance data, the quantum audio magnetotellurics (QAMT) system was developed. This system measures horizontal airborne magnetic fields and horizontal electric fields at the base station (Larnier et al., 2021). MobileMT (MobileMT) measures comparable fields to QAMT and outputs the data as apparent conductivities via internally computing the determinant of the admittance tensor (Sattel et al., 2019).

Available literature offering analysis of the factors that influence airborne NSEM data and inversion results remains sparse. This is especially true for systems that measure electric fields at the base station; e.g. a fundamental analysis of the differences between MT and QAMT impedances. We do know from several studies (Sattel et al., 2019; Holtham, 2012; others) that both ZTEM and MobileMT inversion results are significantly impacted by the choice in starting model. However, because the signals contained with airborne NSEM data are unique to each system, it would be worthwhile to compare inversion results across multiple systems for the same set of inversion parameters.

Our work starts by characterizing the signals present in airborne NSEM data for a base station that measures electric fields; for similar analysis of ZTEM data, see (Lo and Zang, 2008; Holtham, 2012). We discuss the nature of QAMT impedance data before simulating and

comparing MT and QAMT data over a conductor and a resistor. Numerical simulation is then used to characterize the impact of the conductivity at the base station on 3D ZTEM and QAMT anomalies. Unconstrained inversion is used to demonstrate how ZTEM and QAMT inversion results are influenced when the conductivity at the base station differs significantly from the host conductivity within the survey region. Inversion is performed using the conductivity at the base station as the starting and reference models. Then the true host conductivity within the survey region is used as the starting and reference models.

<center>NATURE OF QAMT IMPEDANCES</center>

Defining the QAMT impedance tensor

Starting from the 2x2 impedance tensor that defines MT data (Holtham, 2012), we derive an expression for the 2x2 impedance tensor defining QAMT data. For MT, the impedance tensor is defined as:

$$\begin{bmatrix} Z_{xx} & Z_{xy} \\ Z_{yx} & Z_{yy} \end{bmatrix} = \begin{bmatrix} E_x^{(x)} & E_x^{(y)} \\ E_y^{(x)} & E_y^{(y)} \end{bmatrix} \begin{bmatrix} H_x^{(x)} & H_x^{(y)} \\ H_y^{(x)} & H_y^{(y)} \end{bmatrix}^{-1} \quad (1)$$

where impedances Z_{ij} define the relationships between horizontal electric and magnetic fields for 2 incident planewave polarizations; denoted by superscripts (x) and (y). Expression (1) implies that anomalies observed in the MT impedance data depend on spatial variations in both electric and magnetic field measurements throughout the survey area. Let us now restate expression (1) more concisely as:

$$Z = E_{rx} H_{rx}^{-1} \quad (2)$$

where the subscript rx refers to a non-stationary receiver location. When collecting QAMT data, the electric fields used to compute the impedances are measured at a base station (Larnier, et al., 2021). We therefore define the 2x2 impedance tensor for QAMT as:

$$Q = E_b H_{rx}^{-1} \quad (3)$$

where subscript b refers to fields measured at the base station. We let Q_{ij} denote the QAMT impedances within the tensor. Using expression (2) and (3), we obtain:

$$Q = E_b E_{rx}^{-1} E_{rx} H_{rx}^{-1} = E_b E_{rx}^{-1} Z \quad (4)$$

According to expression (4), QAMT impedances are equivalent to removing the direct influence of spatial variation in the electric field from MT impedances and normalizing the quantity by the electric fields measured at

the base station. We therefore expect the shape and location of anomalies within QAMT impedance data to be primarily driven by anomalous magnetic fields within the survey area. And electric fields act as more of a scaling factor for QAMT anomalies.

Numerical Simulation for a Synthetic Model

To better understand expression (4), we use SimPEG (Heagy, et al., 2017) to simulate the NSEM fields and impedances for a model consisting of a conductor (0.01 S/m) and a resistor (0.0001 S/m) within a halfspace (0.001 S/m); see Figure 1. We quantify the change in amplitude and phase experienced by the NSEM fields due to the conductor and resistor for an incident planewave polarization along the x-direction, relative to the fields for a 0.001 S/m halfspace. We then examine MT and QAMT anomalies to determine whether they are driven by anomalous electric or magnetic fields.

Electric and magnetic fields are simulated at the Earth's surface for both the block and halfspace models. Both the conductor and resistor are buried at a depth of 300 m, and have dimensions 2000 m x 600 m x 500 m. The simulated fields are then used to compute Z_{xy} and Q_{xy} impedances. In this paper, all fields and impedances are simulated using a $-i\omega t$ Fourier convention with X = Northing, Y = Easting and Z +ve downward.
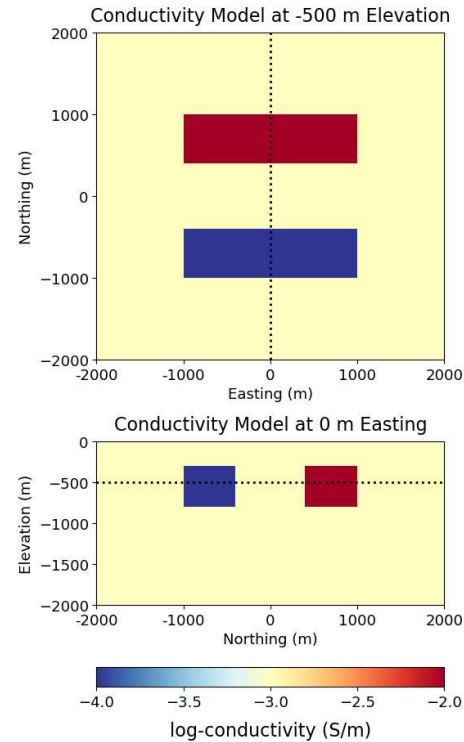
Figure 1. Conductivity model.

For our analysis, we consider fields $E_x^{(x)}$ and $H_y^{(x)}$, as defined in expression (1), and impedances Z_{xy} and Q_{xy}. To characterize the impact of the conductor and resistor on the amplitudes, we compute the percent amplitude difference. I.e.:

$$\% \text{ ampl. diff.} = 100\% \times \left(\frac{|f(\sigma_{block})| - |f(\sigma_{hs})|}{|f(\sigma_{hs})|} \right) \quad (5)$$

And for the phase, we compute the difference in amplitude. I.e.

$$\text{Phase diff} = |\varphi(\sigma_{block})| - |\varphi(\sigma_{hs})| \quad (6)$$

In Figure 2, we illustrate the impact of the conductor and resistor on the amplitudes of $E_x^{(x)}$ and $H_y^{(x)}$, Z_{xy} and Q_{xy} at 360 Hz. And in Figure 3, we illustrate the impact on the phase at 360 Hz. Comparing Figures 2a and 3a to Figures 2b and 3b, we see that anomalous electric fields produce much stronger and more compact signatures than anomalous magnetic fields in both amplitude and phase. Therefore, natural source electric fields are much

more impacted by confined structures than magnetic fields. When examining the size and location of the signatures in Figures 2c and 3c, we see that signatures in Z_{xy} are highly correlated with those in $E_x^{(x)}$ (Figures 2a and 3a) and effectively uncorrelated with those in $H_y^{(x)}$ (Figures 2b and 3b); implying anomalous electric fields are almost entirely responsible for anomalous signatures in MT impedance data. However, when examining the size and location of signatures in Figures 2d and 3d, we see that signatures in Q_{xy} are highly correlated with those in $H_y^{(x)}$ (Figures 2b and 3b) and uncorrelated with those in $E_x^{(x)}$ (Figures 2a and 3a). This supports our assertion following expression (4) that the shape and amplitude of QAMT impedance anomalies are primarily driven by anomalous magnetic fields within the survey region.
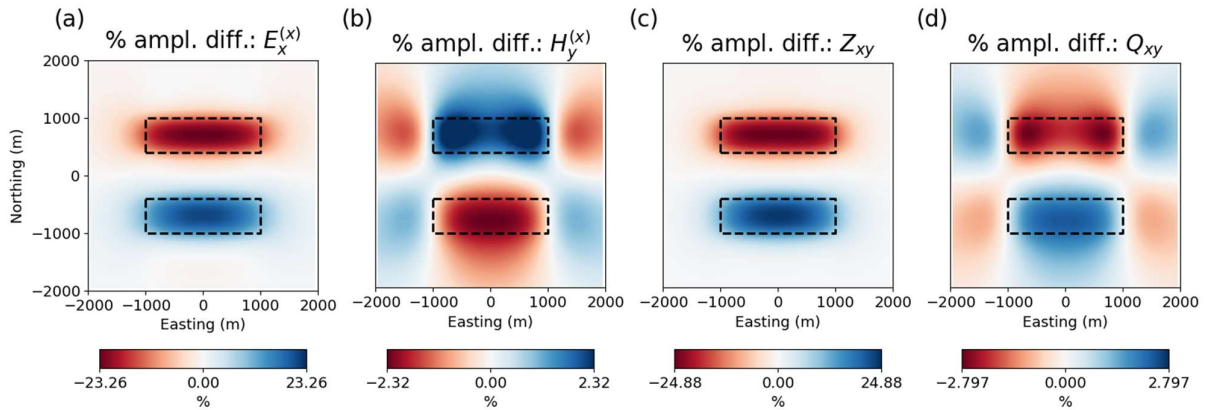
Figure 2. % amplitude difference at 360 Hz for (a) $E_x^{(x)}$, (b) $H_y^{(x)}$, (c) Z_{xy} and (d) Q_{xy}.
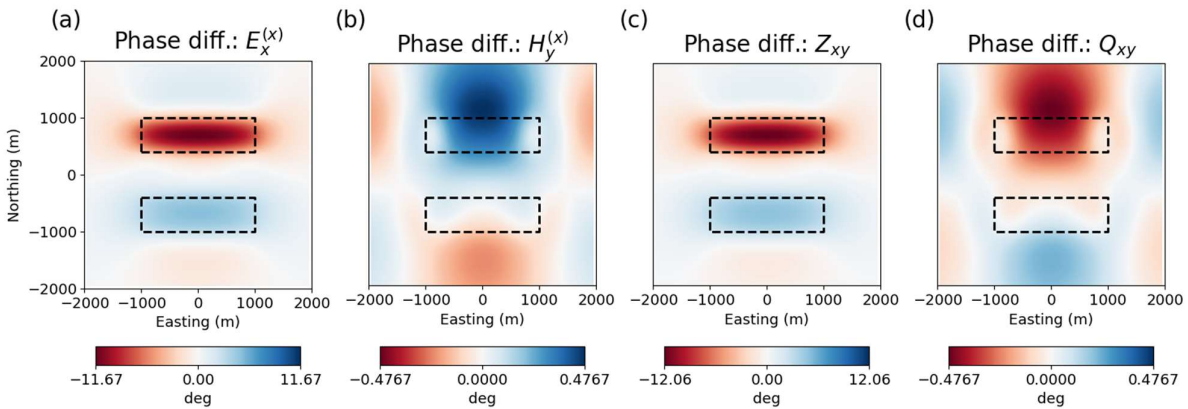
Figure 3. Phase difference at 360 Hz for (a) $E_x^{(x)}$, (b) $H_y^{(x)}$, (c) Z_{xy} and (d) Q_{xy}.

INFLUENCE OF BASE STATION CONDUCTIVITY ON AIRBORNE NSEM ANOMALIES

Base station conductivity defines the conductivity within the region that influences field measurements at the base station. Here, we characterize the influence of the base station conductivity on ZTEM and QAMT anomalies due to 3D structures within the survey region. Magnetic fields are simulated for the block model illustrated in Figure 1; wherein a conductor (0.01 S/m) and a resistor (0.0001 S/m) are buried within a 0.001 S/m host. Assuming the base station is sufficiently far away from the survey region, and that the NSEM fields at the base station can be characterized by a local halfspace, we simulate the horizontal electric and magnetic fields for halfspace conductivities of 0.0001 S/m, 0.001 S/m and 0.01 S/m. From the simulated fields, QAMT impedances are computed according to expression (4) and ZTEM data are computed according to (Holtham, 2013):

$$\begin{bmatrix} T_{zx} \\ T_{zy} \end{bmatrix} = \begin{bmatrix} H_x^{(x)} & H_x^{(y)} \\ H_y^{(x)} & H_y^{(y)} \end{bmatrix}_b^{-1} \begin{bmatrix} H_z^{(x)} \\ H_z^{(y)} \end{bmatrix}_{rx} \quad (7)$$

In Figure 4, we show the real and imaginary components of T_{zy} at 360 Hz for base station conductivities of 0.0001 S/m, 0.001 S/m and 0.01 S/m. We see the shape and amplitude of the anomalies in the tipper plots is consistent regardless of the base station conductivity. Thus in the absence of 3D structure at the base station, ZTEM data provide information solely about structures within the survey region.

In Figure 5, we show the real and imaginary components of Q_{xy} impedance data at 360 Hz for base station conductivities of 0.0001 S/m, 0.001 S/m and 0.01 S/m. Each time the base station conductivity is increased by a factor of 10, both the real and imaginary components of Q_{xy} are decreased by roughly a factor of $\sqrt{10}$, implying the amplitudes of QAMT impedances are proportional to the inverse square-root of the base station conductivity.

INVERSION USING BASE STATION CONDUCTIVITY

Here, we examine how ZTEM and QAMT inversion results are impacted when the base station conductivity differs significantly from the host conductivity within the survey region. Synthetic data are generated and inverted using the UBC-GIF E3DMT v2 code (Shekhtman, et al., 2023). The code uses a weighted least-squares approach (Li and Oldenburg, 1996), which minimizes an objective function of the form:

$$\varphi(m) = \varphi_d(m) + \beta\varphi_m(m) \quad (8)$$

The data misfit φ_d is 2-norm the weighted residual between observed and predicted data for a model m. And
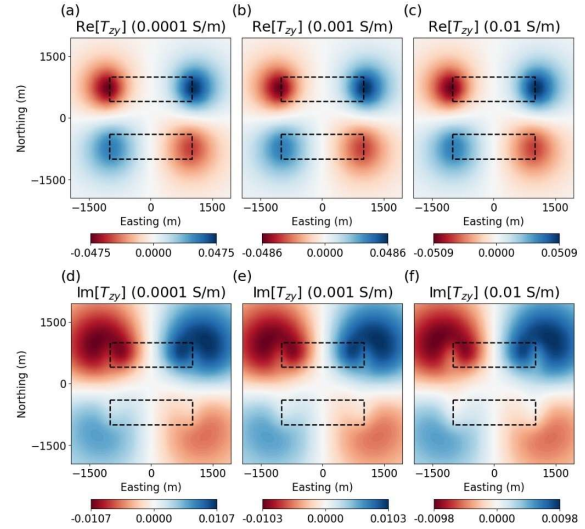
Figure 4. Real and imaginary components of Tzy at 360 Hz for base station conductivities of 0.0001 S/m, 0.001 S/m and 0.01 S/m.
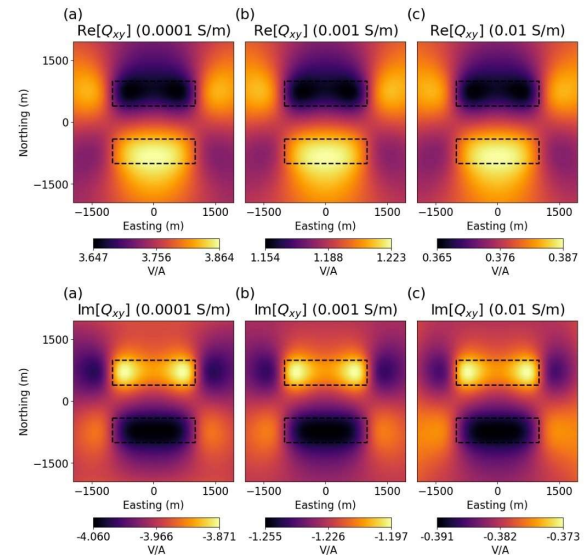
Figure 5. Real and imaginary components of Qxy at 360 Hz for base station conductivities of 0.0001 S/m, 0.001 S/m and 0.01 S/m.

β is the trade-off parameter that balances the data misfit and regularization given by:

$$\varphi_m(m) = \alpha_s \int w_s \, |m\text{-}m_{ref}|^2 dv$$
$$+ \sum_{x,y,z} \alpha_i \int w_i \left| \frac{\partial m}{\partial \gamma_i} \right|^2 dv \quad (9)$$

Constants α_i weight the relative contributions of the smallness and smoothness terms, m_{ref} is the reference model, and w_i are user-defined weighting functions.

For this exercise, we assume that the base station conductivity is known and is used to set the starting and reference models for the inversion. And to reduce the impact of the reference model, we set $\alpha_s = 10^{-10}$ and $\alpha_x = \alpha_y = \alpha_z = 1$.

The model we intend to recover within the survey region was illustrated in Figure 1 and consists of a conductor (0.01 S/m) and a resistor (0.0001 S/m) buried within a 0.001 host. Synthetic QAMT data are generated at frequencies of 45 Hz, 90 Hz, 270 Hz, 720 Hz and 2160 Hz. Synthetic ZTEM data are generated for the first 4 frequencies. The base station used to generate both QAMT and ZTEM data is located at (-30000, 0, 0). Synthetic QAMT and ZTEM data are generated for base station conductivities of 0.0001 S/m, 0.001 S/m and 0.01 S/m; wherein these conductivities are assigned to all cells within 2 skin depths of the base station at the lowest frequency.

In Figure 6, we show the recovered models from ZTEM inversion due to different base station conductivities. These cases represent the outcomes when the base station conductivity is known and assumed to be equal to the host conductivity. When the base station conductivity is equal to the host conductivity (Figure 6b), ZTEM inversion recovers the conductor and resistor appropriately. For a base station conductivity of 0.0001 S/m (Figure 6a), the conductor and the top of the resister

are recovered at much larger depths. And the recovered background conductivity is approximately equal to the base station conductivity. For a base station conductivity of 0.01 S/m (Figure 6c), the conductor and resister are recovered at the surface. And the recovered background conductivity is approximately equal to the base station conductivity.

In Figure 7, we show the recovered models from QAMT inversion due to different base station conductivities. These cases represent the outcome when apparent conductivities computed from QAMT impedances are directly used to choose starting and reference models. When the base station conductivity is equal to the host conductivity (Figure 7b), QAMT inversion recovers the conductor and resistor at appropriately. For a base station conductivity of 0.0001 S/m (Figure 7a), the conductor and the top of the resister are recovered at much larger depth. And the recovered background conductivity is approximately equal to the base station conductivity. For a base station conductivity of 0.01 S/m (Figure 7c), the conductor and resister are recovered at the surface. And the recovered background conductivity is approximately equal to the base station conductivity.

This exercise shows that despite collecting MT-like impedances, QAMT inversion suffers from the same challenges as ZTEM inversion; i.e. that over/underestimation of the starting and reference
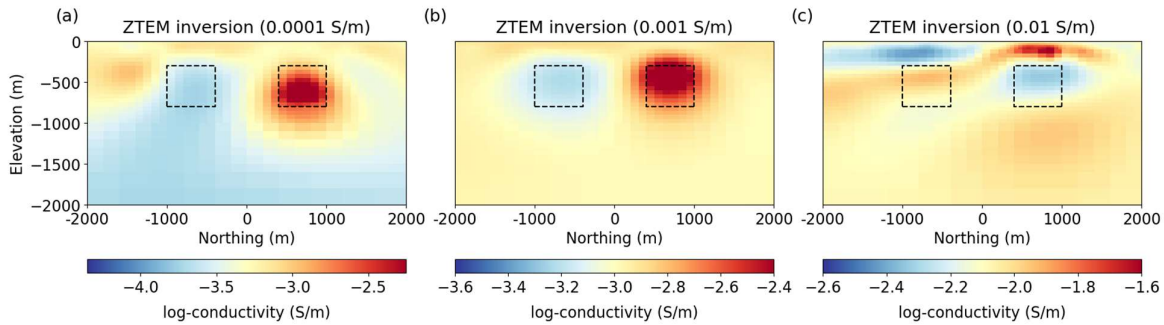
Figure 6. Models from ZTEM inversion where the base station conductivity is used as the starting and reference models: (a) 0.0001 S/m, (b) 0.0001 S/m and (c) 0.01 S/m.
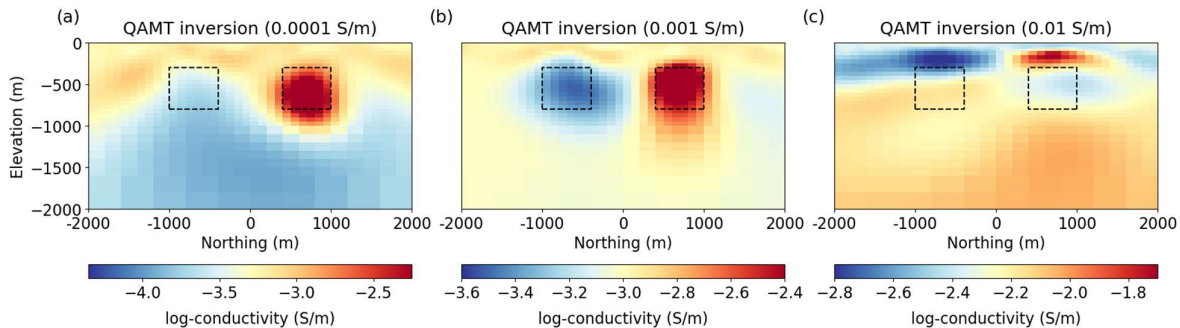
Figure 7. Models from QAMT inversion where the base station conductivity is used as the starting and reference models: (a) 0.0001 S/m, (b) 0.0001 S/m and (c) 0.01 S/m.

models will lead to the recovery of conductors and resistors at erroneous depths. And that choosing a starting and/or reference model directly from apparent conductivities, which are directly sensitivity to the base station conductivity, may not be advisable for QAMT inversion.

INVERSION USING HOST CONDUCTIVITY

Here, we illustrate the ZTEM and QAMT inversion results for different base station conductivities when the true host conductivity within the survey region is known and is used as the starting and reference models.

In Figure 8, we show the recovered models from ZTEM inversion within the survey region due to different base station conductivities. Regardless of the base station conductivity, structures are recovered consistently and at the appropriate depths when the true host conductivity is used as the starting and reference models. Furthermore, the recovered background conductivity is approximately equal to the true host conductivity of 0.001 S/m. Similar results are observed in Figure 9, where we show the recovered models from QAMT inversion within the survey region due to different base station conductivities. Compared ZTEM, QAMT inversion results show a higher contrast in conductivity between recovered structures and the host. However, there also appears to be a little more variation in the recovered models.

In Figure 10, we show the recovered models from ZTEM inversion near the base station. Here, the inversion appears to recover smooth 3D resistive structures, regardless of the true base station conductivity. In Figure 11, we show the recovered models from QAMT inversion near the base station. When the base station conductivity and host conductivity within the survey region are equal, there is no structure recovered at the base station. However when the base station conductivity and host conductivity differ significantly, the inversion recovers significant structure near the base station.

DISCUSSION

Our work started by characterizing the signals present in airborne NSEM data for a base station that measures electric fields. Like ZTEM, QAMT anomalies were shown to result from anomalous magnetic fields produced by 3D structures within the survey region, which are then scaled by field measurements at the base station. And compared to MT impedance anomalies, QAMT impedance anomalies are smaller in amplitude. Assuming the fields at the base station are characterized by a conductive halfspace, we showed that the amplitudes of QAMT impedances are inversely proportional to the square-root of the base station conductivity. We however expect the relationship between QAMT anomalies and the base station conductivity to be more complicated in the presence of 3D structures near the base station.

Recovered models from weighted least-squares inversion of ZTEM and QAMT data are both highly dependent on the starting and reference models. We showed that when the base conductivity differs from the host conductivity and is used as the starting and reference models, structures recovered from airborne NSEM inversion are placed at erroneous depths. However when the true host conductivity is used as the starting and reference models, the inversion of airborne NSEM data recovers consistent structures within the survey region at appropriate depths.

Because EM data are sensitive to cells in proximity of receivers, airborne NSEM inversion is likely to recover structure near the base station. These structures influence the predicted magnetic and electric fields measured at the base station, and thus play a significant role in fitting the data. If structures recovered near the base station play a sufficient role in fitting the shape and amplitudes of airborne NSEM anomalies, we may have reduced confidence in the structures that are recovered within the survey region. Further investigation is needed to characterize the impact of structures recovered near the base station on our interpretation of the inversion result.

CONCLUSION

Airborne NSEM data are effective at identifying 3D conductors and resistors within the survey area by the anomalous magnetic fields they produce. However, these methods are not directly sensitive to the subsurface conductivity within the survey region. When a-priori knowledge of the host conductivity within the survey region is known, both QAMT and ZTEM inversion are effective at recovering conductive and resistive structures within the region of interest. However, unconstrained QAMT and ZTEM inversion is likely to recover structures near the base station that play a significant role in fitting the observed data. This in turn decreases our confidence in the structures recovered within the survey region. All things considered, airborne NSEM methods are much more economical that MT methods and show great promise in being used for a wide range of geophysical applications. And it would be worthwhile to research improvements to inversion methodologies and survey design that includes the collection of airborne NSEM data.
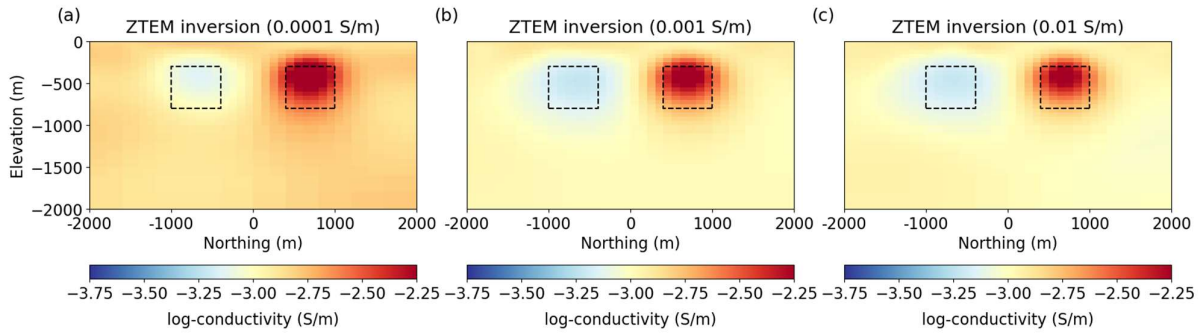
Figure 8. Models from ZTEM inversion within the survey region when the host conductivity is used as the starting and reference models. Base station conductivities of (a) 0.0001 S/m, (b) 0.0001 S/m and (c) 0.01 S/m.
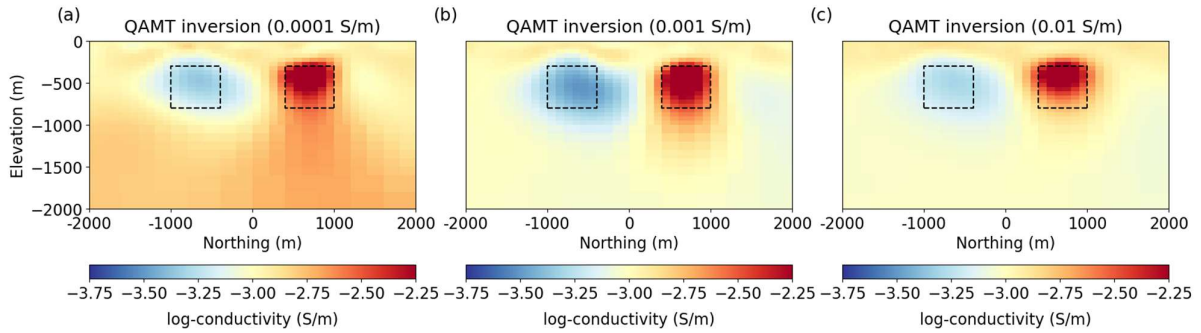
Figure 9. Models from QAMT inversion within the survey region when the host conductivity is used as the starting and reference models. Base station conductivities of (a) 0.0001 S/m, (b) 0.0001 S/m and (c) 0.01 S/m.
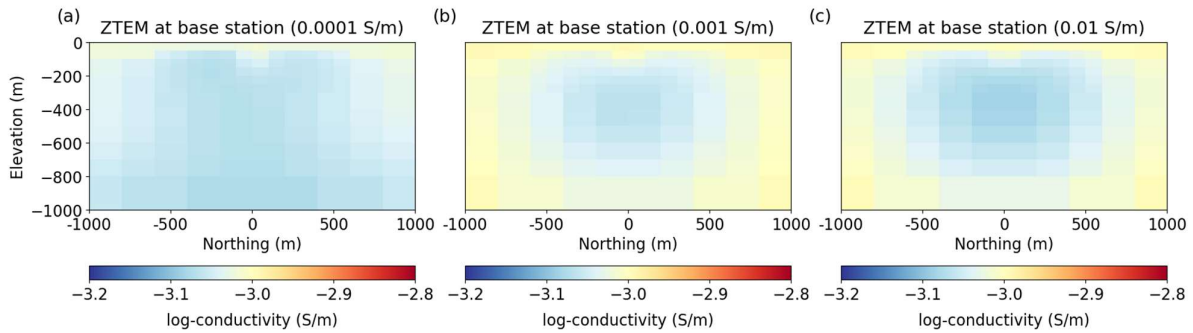
Figure 10. Models from ZTEM inversion near the base station (Easting = -30,000 m) when the host conductivity is used as the starting and reference models. Base station conductivities of (a) 0.0001 S/m, (b) 0.0001 S/m and (c) 0.01 S/m.
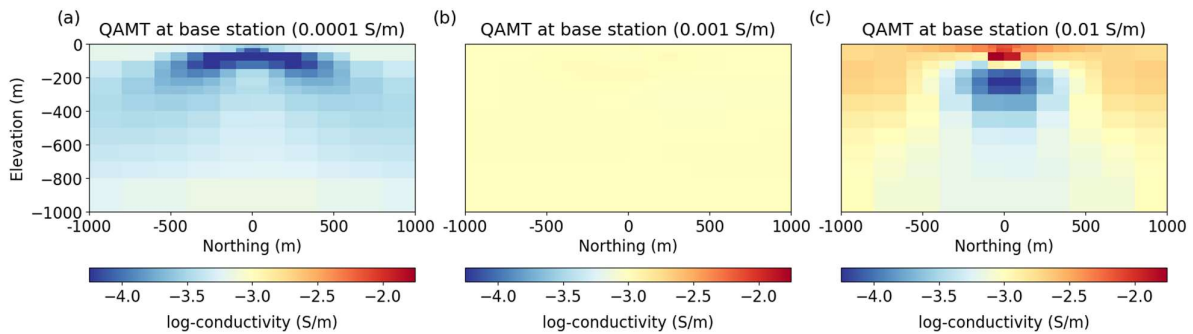
Figure 11. Models from QAMT inversion near the base station (Easting = -30,000 m) when the host conductivity is used as the starting and reference models. Base station conductivities of (a) 0.0001 S/m, (b) 0.0001 S/m and (c) 0.01 S/m.

REFERENCES

Cagniard, L. (1953). Basic Theory of the Magneto-Telluric Method of Geophysical Prospecting. In *Geophysics,* Volume 18, 605–635.

Heagy, L. J., Cockett, R., Kang, S., Rosenkjaer, G. K., and Oldenburg, D. W. (2017). A framework for simulation and inversion in electromagnetics, *Computers & Geosciences*, Volume 107, 1-19, ISSN 0098-3004, http://dx.doi.org/10.1016/j.cageo.2017.06.018.

Holtham, E. (2013). Inversion of Natural Source Electromagnetic Data, *PhD dissertation*, University of British Columbia.

Larnier, H., Chubak, G., Schneider, M., Schiffler, M., and Stolz, R. (2021). Three component SQUID-based system for airborne natural field electromagnetics, *SEG Technical Program Expanded Abstracts*, 1290-1294.

Li, Yaoguo & Oldenburg, D. W. (1996). 3-D inversion of magnetic data. *Geophysics*, Volume 61, 394-408.

Lo, B., and M. Zang (2008). Numerical modeling of Z-TEM (airborne AFMAG) responses to guide exploration strategies, *SEG Technical Program Expanded Abstracts*, Volume 27, 1098–1102.

Sattel, D., Witherly, K. and Kaminski, V. (2019). A brief analysis of MobileMT data, *SEG Technical Program Expanded Abstracts*, 2138-2142.

Tikhonov, A. N. (1950). The determination of the electrical properties of deep layers of the earth's crust, *Doklady. Academii Nauk, SSR,* Volume 73, 295–297.

Shekhtman, R., Oldenburg, D.W., and Haber, E. (2023) E3DMT v2; A Program Library for Forward Modelling and Inversion of Natural Source Electromagnetic Data over 3D Structures. Developed under the consortium research project *Inversion Research Consortium II*, UBC-Geophysical Inversion Facility, Department of Earth and Ocean Sciences, University of British Columbia, Vancouver, British Columbia.

Ward, S. H. (1959). AFMAG – Airborne and ground, *Geophysics*, Volume 24, 761-789.